ELSEVIER

15 September 1995

OPTICS COMMUNICATIONS

Optics Communications 119 (1995) 682–692

Full length article

Nearly-degenerate frequency technique for simultaneous measurement of $n^{(2)}$ and $\alpha^{(2)}$, and four-wave mixing gain coefficients in waveguides

R.P. Espindola, M.K. Udo, S.T. Ho

Department of Electrical Engineering and Computer Science, Northwestern University, Evanston, IL 60208, USA

Received 22 September 1994; revised version received 26 June 1995

Abstract

We describe an experimental technique that allows the simultaneous measurement of the nonlinear refractive index $n^{(2)}$ and the nonlinear absorption coefficient $\alpha^{(2)}$ in waveguides. With minor modifications in the experimental setup, the four-wave mixing gain coefficient can also be measured. Measurements are demonstrated in AlGaAs waveguides.

1. Introduction

Several techniques have been used to investigate the nonlinear refractive index $n^{(2)}$ and the nonlinear absorption coefficient $\alpha^{(2)}$ of materials. The Z-scan technique [1] based on beam self-focusing has been used to measure $n^{(2)}$ and $\alpha^{(2)}$ in samples of glass and semiconductors. Although this technique is simple and sensitive, it is not applicable to waveguides. In waveguides, both fringe-shift interferometry [2,3] and pulsed-modulated interferometry [4] have been used to directly measure $n^{(2)}$ and $\alpha^{(2)}$, while time division interferometry [5] and heterodyne pump-probe [6] have been used to measure the dynamics of $n^{(2)}$ and $\alpha^{(2)}$ in devices such as laser diodes and laser amplifiers. In addition, nondegenerate four-wave mixing has been used to measure the imaginary component and absolute magnitude of $\chi^{(3)}$ [7]. In this paper, we describe a measurement technique that allows the simultaneous measurement of $n^{(2)}$ and $\alpha^{(2)}$ in waveguides. This technique also allows the electronic and thermal contributions to $n^{(2)}$ to be determined separately. With minor modifications in the experimental setup, the four-wave mixing (FWM) gain coefficient can also be measured. As will be shown in the next section, for beams with nearly-degenerate frequencies the FWM gain coefficient is related to the optical nonlinearities $n^{(2)}$ and $\alpha^{(2)}$ by simple expressions. Thus, the measurement of the FWM gain coefficient can be used as an independent measure of the magnitude of $n^{(2)}$ or $\alpha^{(2)}$.

In Section 2 we present a simple derivation of the coupled-wave equations for nearly-degenerate FWM and obtained the relationship between the FWM gain coefficient and the optical nonlinearities $n^{(2)}$ and $\alpha^{(2)}$. The experimental technique is presented in Section 3, as follows: a basic overview of the scheme to measure $n^{(2)}$ and $\alpha^{(2)}$ is first presented in Subsection 3.1; a detailed description of the experimental setup used ofr the measurements is then presented in Subsection 3.2, and the results of the measurements are given in Subsection 3.3. Nonlinear absorption measurements are presented in Section 4, while the experimental setup and the results for four-wave mixing gain coefficient

SSDI 0030-4018(95)00410-6

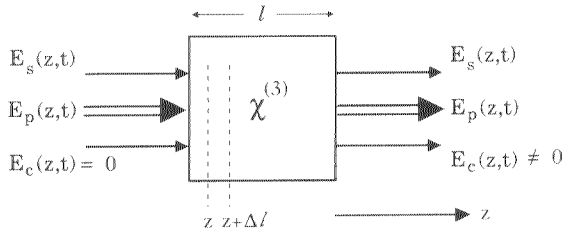

Fig. 1. Nearly-degenerate forward four-wave mixing in a medium with $\chi^{(3)}$ nonlinearity. $E_p(z,t)$ is a strong pump field, $E_s(z,t)$ is the probe field, and $E_c(z,t)$ is the conjugate field.

are presented in Section 5. Finally we present a summary in Section 6.

2. Theoretical background

Here we present a simple derivation of the coupled-wave equations for the case of nearly-degenerate forward FWM and obtain simple relations between the four-wave mixing gain coefficient and $n^{(2)}$ and $\alpha^{(2)}$. Fig. 1 shows the geometry under consideration, where a strong pump field $E_p(z,t)$ with frequency ω_p interacts with a weak probe signal (PSig) field $E_s(z,t)$ with frequency ω_s in a $\chi^{(3)}$ medium of length l, generating a probe conjugate (PConj) field $E_c(z,t)$ with frequency $\omega_c = 2\omega_p - \omega_s$. In the nearly-degenerate case, the frequency difference between the PSig and pump fields satisfies the condition $|\omega_s - \omega_p| < 1/\tau$, where τ is the characteristic response time of the medium's nonlinear refractive index. All four fields are assumed to have the same linear polarization and travel collinearly in the $+z$-direction as would be the case in a waveguide. In this case, the two strong pump fields become spatially degenerate [8,9], and in the steady state, the total field can be written as follows:

$$E_{\text{total}}(z,t) = \varepsilon_p(z)\,e^{-i\omega_p t} + \varepsilon_s(z)\,e^{-i\omega_s t} + \varepsilon_c(z)\,e^{-i\omega_c t}, \quad (1)$$

where $\varepsilon_j(z)$ and ω_j with $j = p, s, c$, are the complex field amplitudes and frequencies of the pump, PSig, and PConj beams, respectively. Inside the medium, the complex field amplitudes of each field at $z + \Delta l$ and z are related by [10] $\varepsilon_j(z+\Delta l) = \varepsilon_j(z)\,e^{ik_j\Delta l}$, where $k_j = (\omega_j/c)(n^{(0)} + n^{(2)}I) + i\,\alpha^{(2)}I/2$, and $n^{(0)}$ is the linear refractive index, $n^{(2)}$ is the nonlinear refractive index, $\alpha^{(2)}$ is the nonlinear absorption coefficient, c is the speed of light in vacuum, and $I(z,t) = E^*_{\text{total}}(z,t)\,E_{\text{total}}(z,t)$ is the total intensity. The explicit expression for $I(z,t)$ can be obtained by using Eq. (1), from which we can see that $I(z,t)$ is time-varying. Using Eq. (1) and $\varepsilon_j(z+\Delta l) = \varepsilon_j(z)\,e^{ik_j\Delta l}$, the total field at $z + \Delta l$ can be written as

$$\begin{aligned} E_{\text{total}}(z+\Delta l,t) &= \varepsilon_p(z+\Delta l)\,e^{-i\omega_p t} \\ &\quad + \varepsilon_s(z+\Delta l)\,e^{-i\omega_s t} + \varepsilon_c(z+\Delta l)\,e^{-i\omega_c t} \\ &= [\,1 + i\omega_p\Delta l(n^{(0)} + n^{(2)}I)/c \\ &\quad - \alpha^{(2)}I\Delta l/2\,]\,\varepsilon_p(z)\,e^{-i\omega_p t} \\ &\quad + [\,1 + i\omega_s\Delta l(n^{(0)} + n^{(2)}I)/c \\ &\quad - \alpha^{(2)}I\Delta l/2\,]\,\varepsilon_s(z)\,e^{-i\omega_s t} \\ &\quad + [\,1 + i\omega_c\Delta l(n^{(0)} + n^{(2)}I)/c \\ &\quad - \alpha^{(2)}I\Delta l/2\,]\,\varepsilon_c(z)\,e^{-i\omega_c t}, \end{aligned} \quad (2)$$

where we have assumed Δl to be small in the second line of Eq. (2) and the exponentials $e^{ik_j\Delta l}$ were expanded in terms of Δl to the first order.

Substituting the explicit expression of $I(z,t)$ into Eq. (2), using $\omega_c = 2\omega_p - \omega_s$, and matching terms with the same temporal dependence in the first and second lines of Eq. (2), leads to three separate equations, which can be written as

$$\begin{aligned} \frac{\varepsilon_p(z+\Delta l) - \varepsilon_p(z)}{\Delta l} &= i\,\frac{\omega_p}{c}n^{(0)}\varepsilon_p(z) \\ &\quad + \left[i\,\frac{\omega_p}{c}n^{(2)} - \frac{\alpha^{(2)}}{2}\right]\varepsilon_p^*(z)\varepsilon_p(z)\varepsilon_p(z), \end{aligned} \quad (3)$$

$$\begin{aligned} \frac{\varepsilon_s(z+\Delta l) - \varepsilon_s(z)}{\Delta l} &= i\,\frac{\omega_s}{c}n^{(0)}\varepsilon_s(z) \\ &\quad + 2\left[i\,\frac{\omega_s}{c}n^{(2)} - \frac{\alpha^{(2)}}{2}\right]\varepsilon_p^*(z)\varepsilon_p(z)\varepsilon_s(z) \\ &\quad + \left[i\,\frac{\omega_s}{c}n^{(2)} - \frac{\alpha^{(2)}}{2}\right]\varepsilon_p(z)\varepsilon_p(z)\varepsilon_c^*(z), \end{aligned} \quad (4)$$

$$\begin{aligned} \frac{\varepsilon_c(z+\Delta l) - \varepsilon_c(z)}{\Delta l} &= i\,\frac{\omega_c}{c}n^{(0)}\varepsilon_c(z) \\ &\quad + 2\left[i\,\frac{\omega_c}{c}n^{(2)} - \frac{\alpha^{(2)}}{2}\right]\varepsilon_p^*(z)\varepsilon_p(z)\varepsilon_c(z) \\ &\quad + \left[i\,\frac{\omega_c}{c}n^{(2)} - \frac{\alpha^{(2)}}{2}\right]\varepsilon_p(z)\varepsilon_p(z)\varepsilon_s^*(z). \end{aligned} \quad (5)$$

In the above equations, we neglected terms that are second-order or higher in the weak probe fields. In the

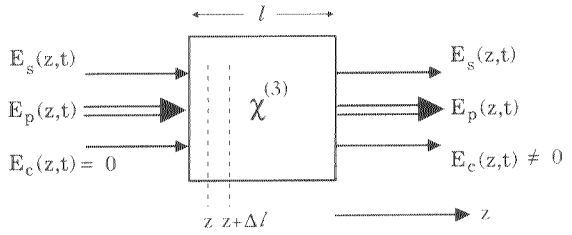

Fig. 1. Nearly-degenerate forward four-wave mixing in a medium with $\chi^{(3)}$ nonlinearity. $E_p(z,t)$ is a strong pump field, $E_s(z,t)$ is the probe field, and $E_c(z,t)$ is the conjugate field.

are presented in Section 5. Finally we present a summary in Section 6.

2. Theoretical background

Here we present a simple derivation of the coupled-wave equations for the case of nearly-degenerate forward FWM and obtain simple relations between the four-wave mixing gain coefficient and $n^{(2)}$ and $\alpha^{(2)}$. Fig. 1 shows the geometry under consideration, where a strong pump field $E_p(z,t)$ with frequency ω_p interacts with a weak probe signal (PSig) field $E_s(z,t)$ with frequency ω_s in a $\chi^{(3)}$ medium of length l, generating a probe conjugate (PConj) field $E_c(z,t)$ with frequency $\omega_c = 2\omega_p - \omega_s$. In the nearly-degenerate case, the frequency difference between the PSig and pump fields satisfies the condition $|\omega_s - \omega_p| < 1/\tau$, where τ is the characteristic response time of the medium's nonlinear refractive index. All four fields are assumed to have the same linear polarization and travel collinearly in the $+z$-direction as would be the case in a waveguide. In this case, the two strong pump fields become spatially degenerate [8,9], and in the steady state, the total field can be written as follows:

$$E_{\text{total}}(z,t) = \varepsilon_p(z)\,e^{-i\omega_p t} + \varepsilon_s(z)\,e^{-i\omega_s t} + \varepsilon_c(z)\,e^{-i\omega_c t}, \quad (1)$$

where $\varepsilon_j(z)$ and ω_j with $j = p, s, c$, are the complex field amplitudes and frequencies of the pump, PSig, and PConj beams, respectively. Inside the medium, the complex field amplitudes of each field at $z + \Delta l$ and z are related by [10] $\varepsilon_j(z+\Delta l) = \varepsilon_j(z)\,e^{ik_j\Delta l}$, where $k_j = (\omega_j/c)(n^{(0)} + n^{(2)}I) + i\,\alpha^{(2)}I/2$, and $n^{(0)}$ is the linear refractive index, $n^{(2)}$ is the nonlinear refractive index, $\alpha^{(2)}$ is the nonlinear absorption coefficient, c is the speed of light in vacuum, and $I(z,t) = E^*_{\text{total}}(z,t)\,E_{\text{total}}(z,t)$ is the total intensity. The explicit expression for $I(z,t)$ can be obtained by using Eq. (1), from which we can see that $I(z,t)$ is time-varying. Using Eq. (1) and $\varepsilon_j(z+\Delta l) = \varepsilon_j(z)\,e^{ik_j\Delta l}$, the total field at $z + \Delta l$ can be written as

$$\begin{aligned} E_{\text{total}}(z+\Delta l,t) &= \varepsilon_p(z+\Delta l)\,e^{-i\omega_p t} \\ &\quad + \varepsilon_s(z+\Delta l)\,e^{-i\omega_s t} + \varepsilon_c(z+\Delta l)\,e^{-i\omega_c t} \\ &= [\,1 + i\omega_p\Delta l(n^{(0)} + n^{(2)}I)/c \\ &\quad - \alpha^{(2)}I\Delta l/2\,]\,\varepsilon_p(z)\,e^{-i\omega_p t} \\ &\quad + [\,1 + i\omega_s\Delta l(n^{(0)} + n^{(2)}I)/c \\ &\quad - \alpha^{(2)}I\Delta l/2\,]\,\varepsilon_s(z)\,e^{-i\omega_s t} \\ &\quad + [\,1 + i\omega_c\Delta l(n^{(0)} + n^{(2)}I)/c \\ &\quad - \alpha^{(2)}I\Delta l/2\,]\,\varepsilon_c(z)\,e^{-i\omega_c t}, \end{aligned} \quad (2)$$

where we have assumed Δl to be small in the second line of Eq. (2) and the exponentials $e^{ik_j\Delta l}$ were expanded in terms of Δl to the first order.

Substituting the explicit expression of $I(z,t)$ into Eq. (2), using $\omega_c = 2\omega_p - \omega_s$, and matching terms with the same temporal dependence in the first and second lines of Eq. (2), leads to three separate equations, which can be written as

$$\begin{aligned} \frac{\varepsilon_p(z+\Delta l) - \varepsilon_p(z)}{\Delta l} &= i\,\frac{\omega_p}{c}n^{(0)}\varepsilon_p(z) \\ &\quad + \left[i\,\frac{\omega_p}{c}n^{(2)} - \frac{\alpha^{(2)}}{2}\right]\varepsilon_p^*(z)\varepsilon_p(z)\varepsilon_p(z), \end{aligned} \quad (3)$$

$$\begin{aligned} \frac{\varepsilon_s(z+\Delta l) - \varepsilon_s(z)}{\Delta l} &= i\,\frac{\omega_s}{c}n^{(0)}\varepsilon_s(z) \\ &\quad + 2\left[i\,\frac{\omega_s}{c}n^{(2)} - \frac{\alpha^{(2)}}{2}\right]\varepsilon_p^*(z)\varepsilon_p(z)\varepsilon_s(z) \\ &\quad + \left[i\,\frac{\omega_s}{c}n^{(2)} - \frac{\alpha^{(2)}}{2}\right]\varepsilon_p(z)\varepsilon_p(z)\varepsilon_c^*(z), \end{aligned} \quad (4)$$

$$\begin{aligned} \frac{\varepsilon_c(z+\Delta l) - \varepsilon_c(z)}{\Delta l} &= i\,\frac{\omega_c}{c}n^{(0)}\varepsilon_c(z) \\ &\quad + 2\left[i\,\frac{\omega_c}{c}n^{(2)} - \frac{\alpha^{(2)}}{2}\right]\varepsilon_p^*(z)\varepsilon_p(z)\varepsilon_c(z) \\ &\quad + \left[i\,\frac{\omega_c}{c}n^{(2)} - \frac{\alpha^{(2)}}{2}\right]\varepsilon_p(z)\varepsilon_p(z)\varepsilon_s^*(z). \end{aligned} \quad (5)$$

In the above equations, we neglected terms that are second-order or higher in the weak probe fields. In the

limit where $\Delta l \to 0$, from Eqs. (3)–(5) we obtain the following three differential equations:

$$\frac{\partial \varepsilon_p'(z)}{\partial z} = i X_R F_p^{(2)} \varepsilon_p'(z)\varepsilon_p'^*(z)\varepsilon_p'(z) - X_I F_p^{(2)} \varepsilon_p'(z)\varepsilon_p'^*(z)\varepsilon_p'(z) , \quad (6)$$

$$\frac{\partial \varepsilon_s'(z)}{\partial z} = i 2 X_R F_s^{(2)} \varepsilon_p'(z)\varepsilon_p'^*(z)\varepsilon_s'(z) - 2 X_I F_s^{(2)} \varepsilon_p'(z)\varepsilon_p'^*(z)\varepsilon_s'(z) + i (X_R + iX_I) F_{sc}^{(2)} \varepsilon_p'(z)\varepsilon_p'(z)\varepsilon_c'^*(z) , \quad (7)$$

$$\frac{\partial \varepsilon_c'(z)}{\partial z} = i 2 X_R F_c^{(2)} \varepsilon_p'(z)\varepsilon_p'^*(z)\varepsilon_c'(z) - 2 X_I F_s^{(2)} \varepsilon_p'(z)\varepsilon_p'^*(z)\varepsilon_c'(z) + i (X_R + iX_I) F_{sc}^{(2)} \varepsilon_p'(z)\varepsilon_p'(z)\varepsilon_s'^*(z) , \quad (8)$$

where $X_R = (\omega/c)n^{(2)}$, $X_I = \alpha^{(2)}/2$, and as discussed below the $F^{(2)}$ coefficients arise when we further average over the waveguide modes. Note that in the nearly-degenerate frequency region, $\omega = \omega_p \sim \omega_s \sim \omega_c$. In addition, the linear phase term has been transformed away via the change of variable $\varepsilon_j(z) = \varepsilon_j'(z) \exp[i \omega_j n^{(0)}/c]$. The equations obtained via our simple derivation agree well with the full-fledge theory in the literature [9]. Following a similar procedure performed by Ho et al. [9], the effect of the waveguide mode profile variation is taken into account by introducing mode overlapping integrals $F_p^{(2)}$, $F_s^{(2)}$, $F_c^{(2)}$, and $F_{sc}^{(2)}$ into the nonlinear terms of the above equations. Let $u_p(x, y)$, $u_s(x, y)$, and $u_c(x, y)$ be the transverse spatial mode profiles of the pump and two probe beams, respectively, then:

$$F_{s,c,p,sc}^{(2)} = \frac{\iint u_{s,c,p,s}(x, y) u_p^2(x, y) u_{s,c,p,c}(x, y)\, dx\, dy}{\iint u_{s,c,p,s}^2(x, y)\, dx\, dy} . \quad (9)$$

If we assume only the lowest order guided-modes, then we can make the following approximations: $u_p(x, y) = u_s(x, y) = u_c(x, y) = \cos(k_x x) \cos(k_y y)$, giving $F_p^{(2)} = F_s^{(2)} = F_c^{(2)} = F_{sc}^{(2)} = 0.5625$, where $k_x = \pi/d_x$, $k_y = \pi/d_y$, and d_x and d_y are the transverse dimensions of the waveguide. The above equations are valid for both continuous-wave beams and pulsed beams with square pulses. Beams with non-square pulses can be treated by dividing each pulse into many small sections and approximating each section with a square pulse.

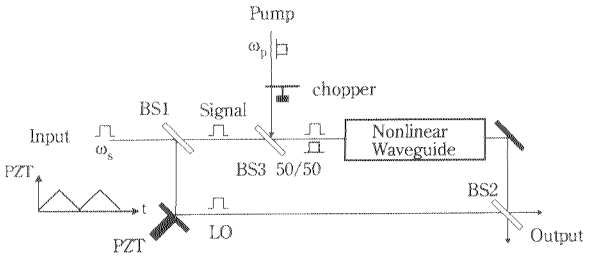

Fig. 2. Schematic of the balanced Mach-Zehnder interferometer, with Signal and LO pulse at frequency ω_s and pump pulse at frequency ω_p.

From Eqs. (6)–(8), it is evident that the pump field experiences nonlinear absorption proportional to X_I and nonlinear phase shift proportional to X_R. The weak PSig and PConj fields experience nonlinear absorption proportional to $2X_R$ and nonlinear phase shift proportional to $2X_I$, which are twice the value experienced by the strong pump field. This factor of two difference exists between the probe and pump fields even in the degenerate frequency limit and is a well-known fact in nonlinear optics [9].

From Eq. (7), we see that $\varepsilon_s'(z)$ is coupled to $\varepsilon_c'^*(z)$ by the four-wave mixing process via coefficient $X = (X_R + i X_I)$, which will be referred to as the FWM gain coefficient. Due to this coupling, a PSig beam injected into the nonlinear medium at frequency $\omega_p - \Delta\omega$ will generate a PConj field at frequency $\omega_p + \Delta\omega$. In the case of a short medium of length Δz, such that $\Delta z\, |X|\, |\varepsilon_p'|^2 < 1$, the solution of Eq. (7) is simply $|\varepsilon_c'/\varepsilon_s'| = |X| F_{sc}^{(2)} |\varepsilon_p'|^2 \Delta z$. In this case, the value of $|X|$ can be easily obtained by measuring the relative magnitudes of the PSig and PConj fields at the waveguide output.

3. Simultaneous measurement of $n^{(2)}$ and $\alpha^{(2)}$ in waveguides

3.1. Basic scheme

In this section we give an overview of the basic ideas behind the measurement scheme and discuss the detection techniques required to measure the parallel and perpendicular components of $n^{(2)}$ and $\alpha^{(2)}$. The

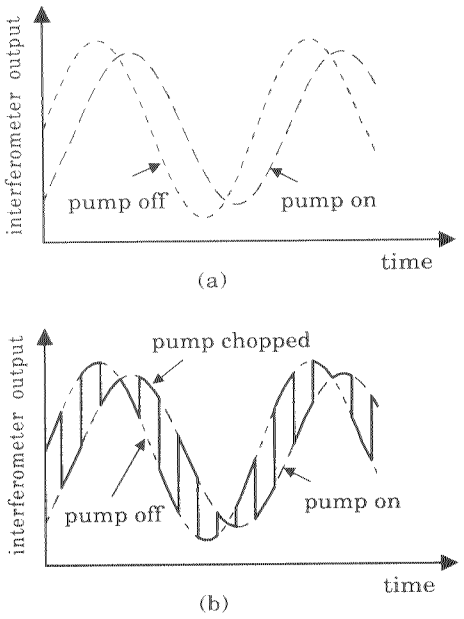

Fig. 3. Illustration of interference between Signal and LO as displayed by an oscilloscope for the cases when: (a) the pump is on (long dash) and off (tiny dash), and (b) the pump is chopped at a rate faster than the PZT ramping.

details of the actual experimental set up for measuring $n^{(2)}$ and $\alpha^{(2)}$ in AlGaAs semiconductor waveguides is given in the next section. The measurement scheme is based on a balanced Mach-Zehnder interferometer shown in Fig. 2, where the nonlinear waveguide is located in one arm of the interferometer. An input beam of frequency ω_s is split at the beam splitter BS1 into two beams, a signal beam and a local oscillator (LO) beam. In the absence of the pump beam, the signal beam traverses the arm containing the waveguide and recombines with the LO beam at beam splitter BS2 where the signal and LO beams interfere. The interference signal has a sinusoidal time variation due to the linear phase change imposed on the LO beam via a piezo-electric transducer (PZT). If the phase of the LO beam has the form: $\phi_{LO} = \omega_{ph}t$, where ω_{ph} depends on the PZT ramping rate, then the interference signal will have the form $\cos(\omega_{ph}t)$. We will refer to this low frequency interference signal as the DC interference signal. When a strong pump beam at frequency ω_p, is turned on and co-propagates with the signal beam inside the nonlinear waveguide, the signal beam experiences both nonlinear phase change and nonlinear absorption (with respect to the case when the strong pump beam is off) due to the presence of the pump. As a consequence, the interference signal out of the interferometer shifts in time and its amplitude is lower, as illustrated in Fig. 3a. As the strong pump beam is turned on and off (using a mechanical chopper for example) at a rate faster than the ramping of the PZT, the interference signal out of the interferometer alternates between the pump on and pump off curves, as illustrated in Fig. 3b (solid curve). In actual measurements, only the alternating interference signal indicated by the solid line in Fig. 3b is detected. By fitting two sinusoidal curves to this signal, for the cases when the pump is on and off, simultaneous measurement of the nonlinear refractive index $n^{(2)}$ and the absorption coefficient $\alpha^{(2)}$ experienced by the signal beam can be made. The amplitude change and phase shift between these two curves are then used to determine the values of $\alpha^{(2)}$ and $n^{(2)}$, respectively. The nonlinear refractive index is given by $n^{(2)} = \lambda\phi_{nl}/(2\pi F_s^{(2)} I_{eff} L)$, where λ is the free space wavelength, ϕ_{nl} is the measured nonlinear phase shift, I_{eff} is the effective peak pump intensity at the center of the transverse waveguide mode profile (it is simply the pump's peak intensity in the waveguide for the case of square pulse), and L is the length of the waveguide. The nonlinear absorption coefficient is given by $\alpha^{(2)} = 2\ln(A_{OFF}/A_{ON})/(F_s^{(2)} I_{eff} L)$, where A_{ON} and A_{OFF} are the amplitudes of the fitted sinusoidal signals when the pump is on and off, respectively [See Appendix A for a detailed derivation].

Using this scheme both the parallel and perpendicular components of $n^{(2)}$ and $\alpha^{(2)}$ can be measured. The parallel components $n_{\parallel}^{(2)}$ and $\alpha_{\parallel}^{(2)}$ are measured when the pump and signal beams entering the waveguide have the same polarization, while the perpendicular components $n_{\perp}^{(2)}$ and $\alpha_{\perp}^{(2)}$ are measured when the pump and signal beams have orthogonal polarizations. Different detection techniques are necessary to measure the parallel and perpendicular components of $n^{(2)}$ and $\alpha^{(2)}$. The reason for this is the need to detect the DC interference between the signal and LO beams separately from the strong pump intensity. In the case when the pump and signal beams have orthogonal polarizations, the pump beam intensity can be easily separated from the signal and LO beams before detection with a polarization beam splitter. Measurement of $n_{\perp}^{(2)}$ and $\alpha_{\perp}^{(2)}$ are then obtained by detecting

the DC interference between the signal and LO beams with an oscilloscope. In this case the pump and signal beams can have the same optical frequency. The measurement of $n_{\parallel}^{(2)}$ and $\alpha_{\parallel}^{(2)}$, on the other hand, is more complicated because in this case the pump and signal beams have the same polarization and the two beams cannot be spatially separated before detection [1]. One way to circumvent this problem is to frequency shift the pump beam, amplitude modulated the PSig beam, and select the beat signal between PSig and LO in the radio frequency domain using a RF spectrum analyser [6]. Since the RF spectrum analyzer displays the magnitude of signals, the intensity interference between the signal and LO beams would now have the form $|\cos(\omega_{ph}t)|$ instead of $\cos(\omega_{ph}t)$. In the next section we describe in detail the experimental set up for measuring $n_{\perp}^{(2)}$ and $\alpha_{\perp}^{(2)}$ and also discuss the necessary changes in the set up for measuring $n_{\parallel}^{(2)}$ and $\alpha_{\parallel}^{(2)}$.

3.2. Experimental setup

Fig. 4 shows a schematic of the experimental set up used for measuring $n_{\perp}^{(2)}$ and $\alpha_{\perp}^{(2)}$ in waveguides. The output of a mode-locked laser is split into two orthogonally polarized pump and PSig beams at the polarization beam splitter PBS1, with the pump power about ten times higher than the PSig power (the amount of power split can be adjusted by the half-wave plate HWP1). Part of the PSig beam is split at the polarization beam splitter PBS2 and becomes the local oscillator (LO) beam. The orthogonally polarized pump and PSig beams are then spatially recombined (i.e. spatially overlapped but still orthogonally polarized) at the polarization beam splitter PBS3 and are subsequently coupled into the waveguide. After propagating through the waveguide, the pump and signal beams are recollimated and send through the polarization beamsplitter PBS4. At PBS4 the pump beam is spatially separated from the signal beam, while the signal beam and the LO beam are spatially recombined. Interference between the LO and the PSig beams is accomplished by passing the beams through the half-wave

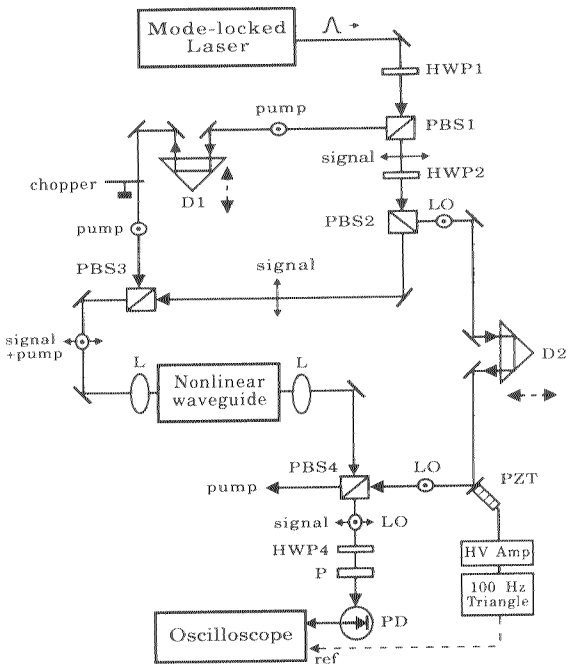

Fig. 4. Schematic of the experimental setup to measure $n^{(2)}$ and $\alpha^{(2)}$ for the case when the pump and Signal beams have the same polarization.

plate HWP3 and the polarizer P. As pointed before, the combination of PBS4, HWP3, and P is equivalent to the beam splitter BS2 in Fig. 2. The phase of the LO beam is linearly varied at 100 Hz via a PZT and the resulting interference between the LO and PSig beams is detected by the photodiode PD and an oscilloscope. As the pump beam is chopped at a rate ($\sim$ 1 kHz) that is faster than the LO phase ramping (100 Hz) the resulting interference signal between the PSig and LO beams alternates between the pump on and pump off states. Two sinusoidal curves are then fitted to the resulting interference trace, one for the pump on case and the other for the pump off case. As mentioned in the previous subsection, the amplitude change and phase difference between these two sinusoidal curves are proportional to $\alpha_{\perp}^{(2)}$ and $n_{\perp}^{(2)}$, respectively. Thus, we see that by using this technique both $n_{\perp}^{(2)}$ and $\alpha_{\perp}^{(2)}$ can be determined simultaneously.

As already discussed in the previous subsection, the measurement of $n_{\parallel}^{(2)}$ and $\alpha_{\parallel}^{(2)}$ requires some modification in the experimental setup in order to frequency shif the pump beam (in the MHz range or higher) and to amplitude modulate the signal beam. The fre-

[1] Such situation does not occur in the homodyne detection where the LO is stronger than the pump and PSig. This is because the strong LO ensures that only the RF beating with the weak signal beam will be picked up (the pump is frequency shifted and has different beat frequency).

quency shift of the pump beam is accomplished by inserting an acousto-optic modulator on the pump beam path, between PBS1 and PBS3, while the amplitude modulation of the signal beam is obtained by inserting a acousto-optical modulator in the signal beam path, between PBS2 and PBS3. The orthogonally polarized pump and signal beams are then spatially recombined at PBS3. The polarizations of the pump and PSig beams are then rotated by 45 degree using a half-wave plate and then the beams are send through a polarizer. After the polarizer, the combined pump and PSig beams have the same polarization, and are subsequently coupled into the waveguide. After going through the waveguide, the pump and PSig beams are send through PBS4, where they are spatially recombined with the orthogonally polarized LO beam. Interference between the PSig and LO beams is accomplished by passing the beams through the half-wave plate HWP3 and the polarizer P, and it is detected by a photodiode and a spectrum analyser. We note that in this case the pump beam will also interfere with the LO beam. However, since the optical frequency of the pump beam has been shifted in the MHz range, the resulting beat signal between the pump and LO beams will also occur in the MHz range. By using a RF spectrum analyser the resulting interference signal between PSig and LO beams is then detected separately from the pump beam [6]. The signal of interest is the DC interference between the LO and PSig beams, which has two components: a slow sinusoidal component (~100 Hz) due to the amplitude interference between the PSig and LO beams, and a fast (~200 kHz) amplitude modulated component resulting from the amplitude modulation on the PSig beam. The spectrum analyzer is tuned to detect the kHz amplitude modulation component and displays the slow (~100 Hz) periodic interference between the PSig and LO beams. In this measurement, the pump beam is also chopped at a rate that is faster than the LO phase ramping, and two curves can be fitted to the data describing the cases when the pump is on and off. We recall that in this case the curves have the form $|\cos|$. The values of $n_{\|}^{(2)}$ and $\alpha_{\|}^{(2)}$ can then be obtained by using the same procedure as described for the perpendicular components.

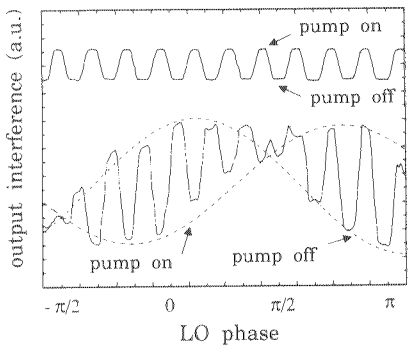

Fig. 5. Nonlinear phase shift and nonlinear absorption data obtained an AlGaAs waveguide using this technique. The data is fitted with two sine envelopes for the cases where the pump is on (solid) and off (dashed). Measurement is made at an RF frequency of 200 kHz.

3.3. Results

We now present the results of our measurements of $n_{\perp}^{(2)}$ and $\alpha_{\perp}^{(2)}$ for a 1 cm long AlGaAs rib waveguide. An additive pulse mode-locked (APM) color-center laser (NaCl:OH) producing 430 fs pulses at 82 MHz repetition rate and with center wavelength at $\lambda \sim 1.6\,\mu$m, was used in these experiments. The AlGaAs epitaxial layers were grown by molecular beam epitaxy (MBE) and consisted of a 5 μm thick $Al_{0.23}Ga_{0.77}As$ guiding region on top of a 2.5 μm thick $Al_{0.60}Ga_{0.40}As$ lower cladding layer grown on a semi-insulating GaAs substrate. The waveguides were patterned via photolithography and chemically etched using H_3PO_4:H_2O_2:H_2O (1:1:35 volume ratios). The height and width of the rib were 2 μm and 4 μm, respectively. The calculated fundamental mode cross-sectional area for this rib waveguide was 4.4 μm by 2.6 μm. Coupling of the laser pulses into and out of the waveguide was done by the end-firing coupling method and in order to minimize losses, both the front and back facets of the waveguide were antireflection coated.

Fig. 5 shows the interference data as displayed on an oscilloscope for the AlGaAs rib waveguide when the pump and signal have orthogonal polarizations. The solid curve corresponds to the intensity interference between PSig and LO beams and the two dashed curves are fitted sinusoidals representing the cases when the pump is on and off. The displacement between the two sinusoidal curves gives the nonlinear

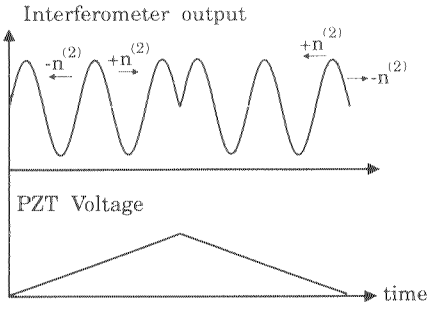

Fig. 6. The upper trace shows the interferometer output signal as function of time, while the lower trace indicates the PZT voltaga as function of time. The arrows indicate the direction in which the interference signal shifts as the pump is turned on for the cases of positive and negatiave $n^{(2)}_{elec}$.

phase shift experienced by the signal due to the pump, and in this case it is approximately $\phi_{nl} = 0.6\pi$. We also measure an 8% decrease in the amplitude of the sinusoidal curve for the pump on case, as compared to that of the pump off case. Using the relations described in Section 3 and estimating the pump power inside the waveguide to be 22 mW, we calculate a nonlinear refractive index $n^{(2)}_{\perp} = 2.1 \pm 0.7 \times 10^{-14}$ cm^2/W and a nonlinear absorption coefficient $\alpha^{(2)}_{\perp} = 0.06 \pm 0.02$ cm/GW. In general, for isotropic materials like AlGaAs the effect of cross-phase modulation (XPM) is 2/3 as strong as that of self-phase modulation (SPM) [11]. Using this fact and comparing the values obtained here for $n^{(2)}_{\perp}$ and $\alpha^{(2)}_{\perp}$ with previously reported values [11,12] of $n^{(2)}_{\parallel} = 3.2 \times 10^{-14}$ cm^2/W and $\alpha^{(2)}_{\parallel} = 0.08$ cm/GW, respectively, we find that our results are in good agreement with them. As can be seen from Fig. 6, the limit of detection for the induced phase shift is approximately $\lambda/20$. The accuracy of the data-fitting is approximately 10%. However, due to errors in the estimation of the pump power and mode area in the waveguide, we estimate that the overall accuracy in determining the nonlinear refractive index and absorption coefficient is probably not better than 35%.

One useful feature of this experimental technique is that it could be used for the determination of both the slow thermal component and the fast electronic component of $n^{(2)}$. The thermal component $n^{(2)}_{thml}$ will be observed in the measurement of $n^{(2)}$ if the thermal response time τ_{thml} of the waveguide material is faster than the turn on time of the pump (i.e. the chopping rate of the pump beam is slower than $1/\tau_{thml}$). Since the electronic component $n^{(2)}_{elec}$ is proportional to peak power and the thermal component $n^{(2)}_{thml}$ is proportional to the average power, it is possible to separate the effect of each other by reducing the pump's average power while keeping the pump peak power constant. By plotting the value of $n^{(2)}$ as a function of the average pump power (peak pump power is kept constant), the value of $n^{(2)}_{elec}$ could then be obtained from this plot in the limit where the average pump power goes to zero. In our experiment we measured the thermal response time of the AlGaAs waveguide and found that at $\lambda \sim 1.6$ μm, for 430 fs pulses at 82 MHz rate, τ_{thml} is about 2 seconds. For materials with long thermal response time like AlGaAs, it is possible to measure the electronic component $n^{(2)}_{elec}$ by chopping the pump beam at a rate faster than the material's thermal response time. The value obtained for $n^{(2)}_{\perp}$ actually corresponds to the electronic component of $n^{(2)}_{\perp}$. The sign of $n^{(2)}_{elec}$ was determined by observing the direction of displacement of the DC interference signal when the pump was turned on, while at the same time observing the direction of the PZT expansion. Fig. 6 illustrates two traces: one is the interferometer output signal as function of time and the other is the PZT voltage as function of time. Here, the arrows indicate the direction in which the interference signal shifts as the pump is turned on for the cases of positive and negative $n^{(2)}_{elec}$. Using this method, we determined that for AlGaAs $n^{(2)}_{elec}$ is positive. This is consistent with recent theoretical and experimental studies of semiconductor optical nonlinearities below the band gap energy [13].

4. Nonlinear absorption measurement

In this section we describe a simpler way to measure the nonlinear absorption coefficient using the same experimental set up as shown in Fig. 4. In this case the nonlinear absorption coefficient is measured by first blocking the LO beam and detecting only the PSig using a detector and oscilloscope. In the absence of the pump beam, the oscilloscope displays the DC level of the PSig beam (i.e., a straight line). When the pump is on, this DC level is reduced due to two-photon absorption of the PSig beam induced by the pump beam. As the pump beam is chopped at kHz

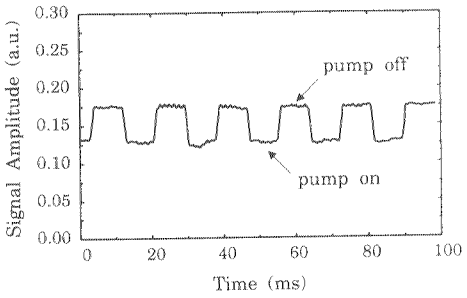

Fig. 7. Trace of the direct measurement of nonlinear absorption for the case when the pump and PSig have orthogonal polarizations.

rate, a periodic trace is obtained showing the PSig beam DC level for the cases when the pump is on and off. Using this technique, we measured $\alpha_{\perp}^{(2)}$ of the same AlGaAs semiconductor waveguide described in Subection 3.3. Fig. 7 shows the periodic trace resulting from two-photon absorption of the PSig beam. In this case, the nonlinear absorption coefficient is given by $\alpha_{\perp}^{(2)} = -\ln[1-(B_{OFF}-B_{ON})/B_{OFF}]/(F_s^{(2)} I_{eff} L)$, where B_{ON} and B_{OFF} are the measured DC level of PSig for the cases of pump on and off, respectively. Estimating the average pump power inside the waveguide to be ~42 mW, we calculate a nonlinear absorption coefficient $\alpha_{\perp}^{(2)} = 0.065 \pm 0.02$ cm/GW, which is in good agreement with the value obtained in Subection 3.3.

5. Four-wave mixing measurement

5.1. Experimental setup

As presented in Section 2, in a forward four-wave mixing (FWM) process a strong pump beam with frequency ω_p interacts with a weak probe signal beam at frequency ω_s in a $\chi^{(3)}$ medium, generating a conjugate beam at frequency $\omega_c = 2\omega_p - \omega_s$. Although four-wave mixing measurements in waveguides have been reported in the literature, here we take advantage of our experimental set up used for $n^{(2)}$ and $\alpha^{(2)}$ measurements to also perform FWM measurements. This is quite convenient since, as shown in Section 2, in the nearly-degenerate frequency region the four-wave mixing (FWM) gain coefficient X is related to $n^{(2)}$ and $\alpha^{(2)}$ by simple expressions. We can therefore use the results of FWM gain coefficient measurement to confirm the value of $n^{(2)}$ or $\alpha^{(2)}$. As already pointed

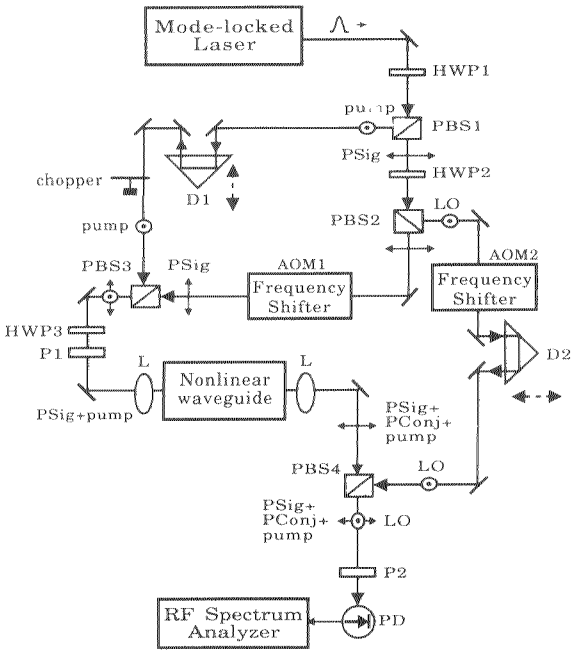

Fig. 8. Schematic of the experimental setup to perform four-wave mixing measurement.

in Section 2, the value of X can be determined from the magnitude of the conjugate and signal beams.

Fig. 8 shows the experimental set up for FWM gain coefficient measurement. In describing this experiment we use the nomenclature established in Section 3 for pump, PSig and LO beams. The pump, PSig and LO beams are obtained from the laser output beam in the same way as described in Subsection 3.2. However, in this experiment, the frequency of the PSig beam is shifted with respect to the frequency of the pump beam, so that the generated conjugate beam, PConj, will have a different optical frequency than that of the pump and PSig beams. This frequency shift is accomplished by passing the PSig beam through the acousto-optic modulator AO1. The orthogonally polarized pump and PSig beams are spatially recombined at the beamsplitter PBS3. After that the polarizations of the pump and PSig beams are rotated by 45 degrees using a half-wave plate and then the beams are send through a polarizer P. The orientation of the polarizer is chosen so that when the pump and PSig beams are coupled into the waveguide they excite only the TM mode. The pump and PSig beams interact inside the $\chi^{(3)}$ nonlinear waveguide, via the

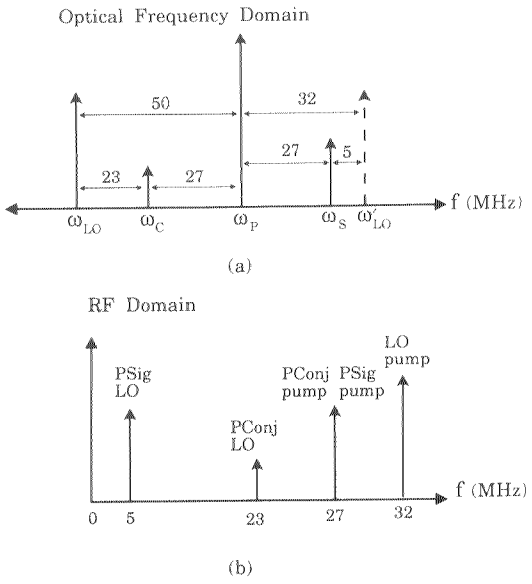

Fig. 9. (a) Optical frequency spectrum of the various beams involved in the four-wave mixing experiment, indicating the frequency shift of the LO, PSIG, and PConj signals with respect to the pump beam; (b) the expected RF beat spectrum in the FWM experiment, with the beating components indicated above each arrow.

FWM process to generate a conjugate beam PConj. At the output of the waveguide, the pump, PSig, and PConj beams are recollimated and sent to the polarization beam splitter PBS4, where they are combined with the frequency shifted LO beam. Using a combination of a half-wave plate and polarizer P2, the pump, PSig, and PConj beams, respectively, interfere with the LO beam, generating three different RF beat signals that are detected using a photodiode and a RF spectrum analyzer (heterodyne detection of the pump, Psig, and PConj beams). We note that the frequency shift of the LO beam should be different than that of the PSig beam so that distinct RF beat signals are obtained. In addition, the amount of frequency shift is chosen so that the RF beat signals occur away from the harmonics of the mode-locked laser frequency.

Fig. 9a shows the optical frequency of the various beams involved in this experiment. Both the PSig and LO beams were frequency shifted with respect to the pump beam. PSig, at frequency ω_S, was up-shifted by 27 MHz, and the LO beam, at ω_{LO}, was down-shifted by 50 MHz. Through the four-wave mixing process,

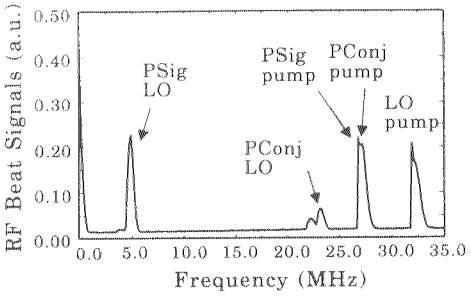

Fig. 10. RF beat signal spectrum resulting from the four-wave mixing experiment in AlGaAs waveguide using 430 fs pulses at $\lambda = 1.6\,\mu$m.

the conjugate beam PConj, at ω_c, was generated at -27 MHz. As indicated in the diagram a second LO signal at ω'_{LO} arises from the pulse repetition rate of the mode-locked laser and differs in frequency from the LO at ω_{LO} by 82 MHz.

Fig. 9b shows the expected beat signals in the RF domain with the beating components indicated above each arrow. Basically, it shows that the 5 MHz signal corresponds to the beating between PSig at ω_S and LO at ω'_{LO}, the 23 MHz signal corresponds to the beating between PConj at ω_C and LO at ω_{LO}, and the 32 MHz signal corresponds to the beating between the pump and the second LO signal (dashed). The 27 MHz signal represents two beating signals: one between the pump and the PSig and the other between the pump and PConj. In the next Subsection we present the experimental results.

5.2. Results

Using the experimental set up described in the previous Subsection, we measured the FWM gain coefficient $|X|$ of the AlGaAs rib waveguide. Fig. 10 shows RF the spectrum resulting from the FWM measurement for the case when the pump and PSig beams have the same polarization. The conditions for the pulse width, pulse center wavelength, and repetition rate were identical to those used for the $n^{(2)}$ and $\alpha^{(2)}$ measurement. As can be seen from Fig. 10, the magnitude of the PConj signal at 23 MHz is about 1/4 of the magnitude of the PSig signal at 5 MHz. As mentioned before, the FWM gain coefficient can be obtained by reading the relative magnitudes of the PSig and PConj fields from the RF spectrum analyzer. Using the estimated values of pump power = 2.4 mW, and the mode

area of 4.5 μm by 2.7 μm, we calculate the four-wave mixing gain coefficient to be $|X| = 8.55 \times 0^{-10}$ cm/W. Since $|X|$ is directly related to $n^{(2)}_{\text{elec}}$ and $\alpha^{(2)}$, it can be used to calculate independently either $n^{(2)}_{\text{elec}}$ or $\alpha^{(2)}$. Using the value obtained for $|X|$ from the FWM measurement and $\alpha^{(2)} = 0.08$ cm/GW, we obtain a value of $n^{(2)} \sim 2.17 \times 10^{-14}$ cm^2/W, which is close to the value obtained earlier using the simultaneous measurement (note that in that case the pump and probe had orthogonal polarizations). We also measured the FWM gain coefficient for the case when the pump and Psig have orthogonal polarizations. In this case, however, the gain coefficient was very small, approaching zero.

6. Summary

In this paper we described a technique that allows simultaneous measurement of $n^{(2)}$ and $\alpha^{(2)}$ in waveguides. Using this technique both the parallel and perpendicular components of $n^{(2)}$ and $\alpha^{(2)}$ can be measured. With some modifications in this experimental set up the FWM gain coefficient can also be measured. We presented results for the measurement of the perpendicular component of $n^{(2)}$ and $\alpha^{(2)}$, and FWM gain coefficient in AlGaAs semiconductor waveguide. Our results for $n^{(2)}$ and $\alpha^{(2)}$ are in reasonable agreement with the values published in the literature. The FWM gain coefficient measurement is used as an independent way to confirm the value obtained for either $n^{(2)}$ or $\alpha^{(2)}$.

Acknowledgements

This work was supported by Advanced Research Project Agency under contract # F30602-92-C-0086-P03.

Appendix A. Derivation of $\alpha^{(2)}$ relation

The expression given in Subsection 3.1 for calculating $\alpha^{(2)}$ is derived here. Although this expression is valid for calculating both $\alpha^{(2)}_{\perp}$ and $\alpha^{(2)}_{\parallel}$, the derivation is slightly different for each case due to the different detection techniques employed. First we present the derivation for the case of $\alpha^{(2)}_{\perp}$. Let the optical powers of LO and PSig beams at the detector be P_{LO} and $P_s = P_0$, respectively. When the pump beam is on, $P_s = P_0 \exp[-\alpha^{(2)}_{\perp} F^{(2)}_s I_{\text{eff}} L]$, where the exponential term is due to two-photon absorption of the PSig beam due to the presence of the orthogonally polarized pump beam. Using the fact that the detector current is given by $I_{\text{Det}} = (\sqrt{P_S} + \sqrt{P_{\text{LO}}})^2$, one can show that the detector current will have an interference term given by

$$I_{\text{inter}} = 2\sqrt{P_{\text{PSig}}}\sqrt{P_{\text{LO}}}\cos(\omega_{\text{ph}} t). \tag{A.1}$$

This term represents the sinusoidal interference between the PSig and LO beams (due to PZT ramping). Let the amplitude of this term be A_{ON} and A_{OFF} for the cases when the pump beam is on and off, respectively. It is easy to show that A_{ON} and A_{OFF} are given by

$$A_{\text{ON}} = 2\sqrt{P_0}\sqrt{P_{\text{LO}}}\exp[-\alpha^{(2)}_{\perp} F^{(2)}_s I_{\text{eff}} L/2], \tag{A.2}$$

$$A_{\text{OFF}} = 2\sqrt{P_0}\sqrt{P_{\text{LO}}}. \tag{A.3}$$

Taking the ratio of A_{ON} and A_{OFF} and solving for $\alpha^{(2)}_{\perp}$ we obtain:

$$\alpha^{(2)}_{\perp} = 2\ln(A_{\text{OFF}}/A_{\text{ON}})/(F^{(2)}_s I_{\text{eff}} L). \tag{A.4}$$

We now present the derivation for $\alpha^{(2)}_{\parallel}$. In this case, $P_s = P_0 + P_M \sin(\omega_M t)$, where $P_M \ll P_0$ is the modulation depth and ω_M is the angular frequency of the kHz amplitude modulation. When the pump beam is on, P_s is given by $P_s = [P_0 + P_M \sin(\omega_M t)] \exp[\alpha^{(2)}_{\parallel} F^{(2)}_s I_{\text{eff}} L]$. The interference term given by Eq. (A.1) has a component oscillating at the kHz frequency, which is then easily selected by the RF spectrum analyzer tuned to detect the amplitude modulation frequency. The RF spectrum analyzer displays the amplitude of this kHz signal given by

$$I^{200\text{kHz}}_{\text{Det}} = P_M\sqrt{P_{\text{LO}}/P_0}\exp[\alpha^{(2)}_{\parallel} F^{(2)}_s I_{\text{eff}} L/2] \times |\cos(\omega_{\text{ph}} t)|, \tag{A.5}$$

where again the exponential term is included only if the pump beam is on. Again let the amplitude of the sinusoidal signal be A_{ON} and A_{OFF} when the pump beam is on and off, respectively. In this case A_{ON} and A_{OFF} are given by

$$A_{\text{ON}} = P_M\sqrt{P_{\text{LO}}/P_0} \times \exp[-\alpha^{(2)}_{\parallel} F^{(2)}_s I_{\text{eff}} L/2], \tag{A.6}$$

$$A_{OFF} = P_M \sqrt{P_{LO}/P_0}. \quad (A.7)$$

Taking the ratio of A_{ON} and A_{OFF} and solving for $\alpha_{\parallel}^{(2)}$ we obtain

$$\alpha_{\parallel}^{(2)} = 2 \ln(A_{OFF}/A_{ON})/(F_s^{(2)} I_{eff} L). \quad (A.8)$$

Comparing the equations for $\alpha_{\perp}^{(2)}$ and $\alpha_{\parallel}^{(2)}$, we see that the equations have the same form.

References

[1] M. Sheik-Bahae, A.A. Said, T.-H. Wei, D.J. Hagan and E.W. Van Stryland, IEEE J. Quantum. Electron. 26 (1990) 760.
[2] D. Cotter, C.N. Ironside, B.J. Ainslie and H.P. Girdlestone, Optics Lett. 14 (1989) 317.
[3] M.C. Gabriel, N.A. Whitaker Jr., C.W. Dirk, M.G. Kuzyk and M. Thakur, Optics Lett. 16 (1991) 1334.
[4] K.B. Rochford, R. Zanoni, G.I. Stegeman, W. Jrug E. Miao and M.W. Beranek, IEEE J. Quant. Elect. 28 (1992) 2044.
[5] M.J. LaGasse, K.K. Anderson, H.A. Haus and J.G. Fujimoto, Appl. Phys. Lett. 54 (1989) 2068.
[6] K.L. Hall, G. Lenz, E.P. Ippen and G. Raybon, Optics Lett. 17 (1992) 874.
[7] H.Q. Le, W.D. Goodhue and K. Rauschenbach, Optics Lett. 15 (1990) 1126.
[8] A. Yariv and R.A. Fisher, in: *Optical Phase Conjugation*, ed. R.A. Fisher (Academic Press, New York, 1983).
[9] S.T. Ho, P. Kumar and J.H. Shapiro, J. Opt. Soc. Am. B8 (1991) 37.
[10] G.J. Milburn, M.D. Levenson, R.M. Shelby, S.H. Perlmutter, R.G. DeVoe and D.F. Walls, J. Opt. Soc. Am. B4 (1987) 1476.
[11] S.T. Ho, C.E. Soccolich, M.N. Islam, W.S. Hobson, A.F.J. Levi and R.E. Slusher, Appl. Phys. Lett. 59 (1991) 2558.
[12] A. Villenueve, C.C. Yang, G.I. Stegeman, C.-H. Lin and H.-H. Lin, Appl. Phys. Lett. 62 (1993) 2465.
[13] M. Sheik-Bahae, D.J. Hagan and E.W. Van Stryland, Phys. Rev. Lett. 65 (1990) 96.